

# Circulation of plasma in the Jupiter's inner magnetosphere revealed from time variation in radial profile of plasma temperature and density obtained by Hisaki/EXCEED observation

\*R. Hikida(1), K. Yoshioka(2), F. Tsuchiya(3), M. Kagitani(3), G. Murakami(4),  
T. Kimura(5), A. Yamazaki(4), and I. Yoshikawa(2)

(1) Department of Earth and Planetary Science, the University of Tokyo,

(2) Department of Complexity Science and Engineering, the University of Tokyo,

(3) Planetary Plasma and Atmospheric Research Center, Tohoku University

(4) Institute of Space and Astronautical Science (ISAS), Japan Aerospace Exploration Agency (JAXA)

(5) Frontier Research Institute for Interdisciplinary Sciences, Tohoku University

# Jovian Magnetosphere

- Due to the fast rotation and strong magnetic field, the corotational electric field is dominant compared to the convective electric field.
- Due to the fast rotation, the centrifugal force is dominant compared to the gravitational force outside  $2 R_J$  from Jupiter.  
→ Corotating plasmas are gradually transported outside.
- Due to the strong magnetic field, drift period is much larger than the rotation period.

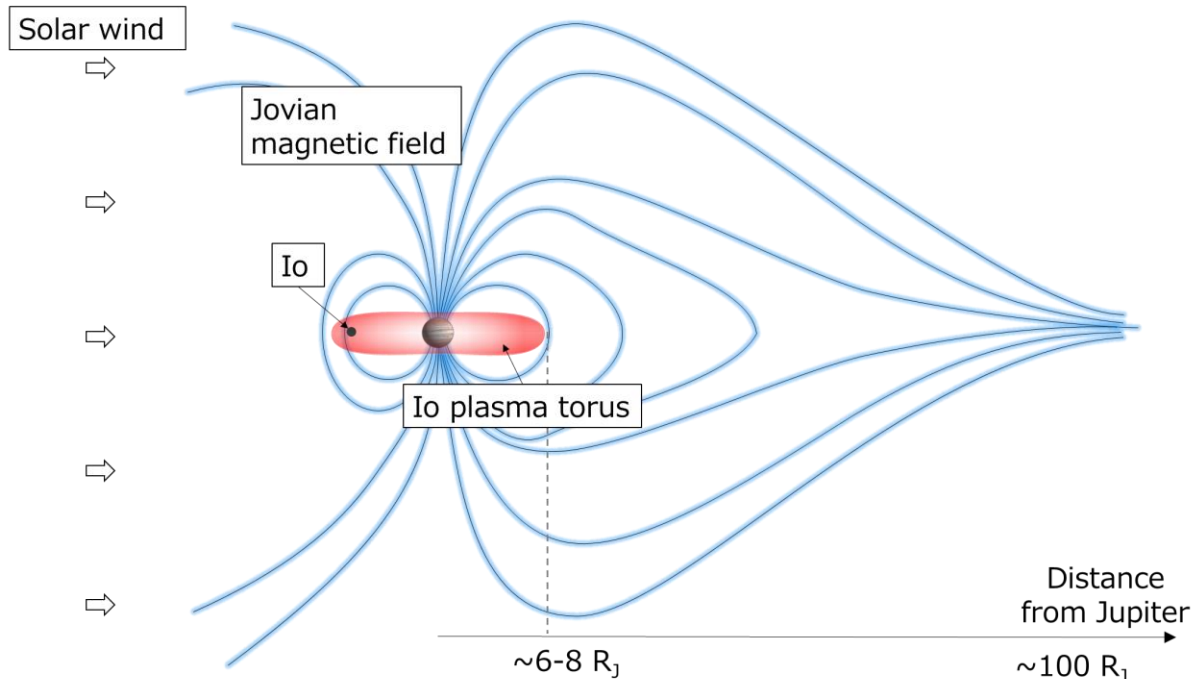


Fig. Schematic view of the Jovian magnetosphere

Table. Comparison between Earth and Jupiter

	Earth	Jupiter
Magnetic moment ( $A \cdot m^2$ )	$8 \times 10^{22}$	$1 \times 10^{26}$
Magnetic field direction at equator	↑	↓
Orbital radius (AU)	1.0	5.2
Plasma source in magnetosphere	×	○
Planetary radius (km)	$6.4 \times 10^3$	$7.2 \times 10^4$
Distance to magnetopause (at noon)	$\sim 10 R_E$	$\sim 100 R_J$
Rotational period (hours)	24	$\sim 10$

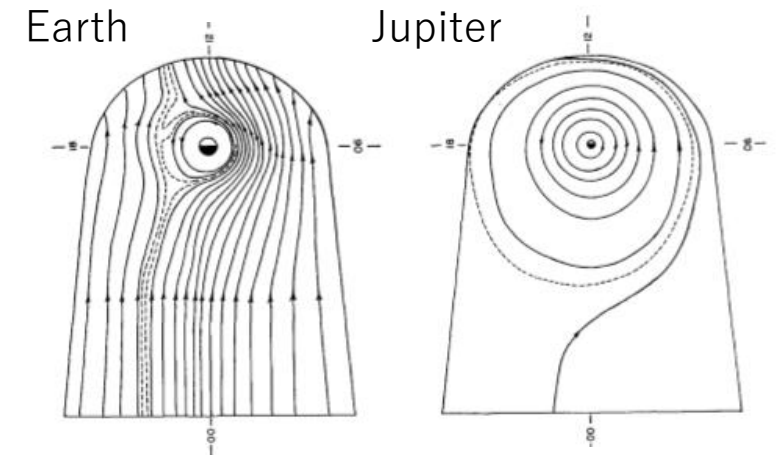


Fig. Schematic diagram of thermal plasma's flow in magnetospheres [Brice and Ioannidis 1970]

# Energy source of radiation from the Io plasma torus (IPT)

- Io's volcanic gas gets caught by the Jupiter magnetic field and picked up. Electrons obtain energy by coulomb collision with ions, and ions emit light mainly in the UV range by collisional excitation with electrons.
- It is impossible to cover the radiation with the pick-up energy alone, and the heating of core electrons (~eV) by hot electrons (~ keV) plays an important role (Delamere & Bagenal, 2003).
- The supply mechanism of hot electrons has not been clarified.**

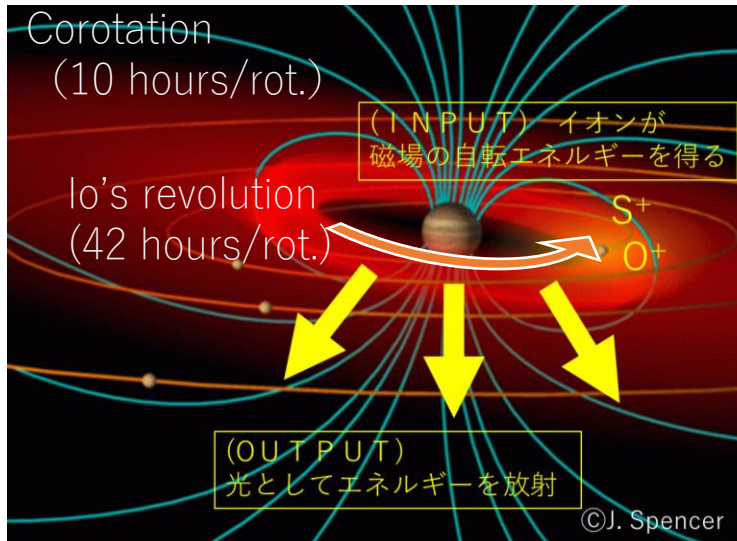


Fig. Schematic view of the IPT



Fig. Gas blows out from volcano on Io caught by Voyager 1

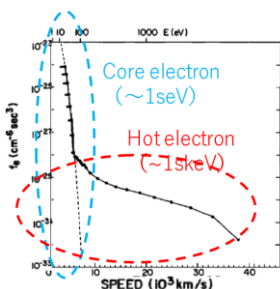
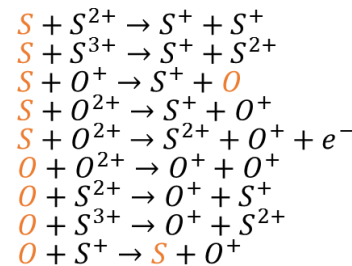
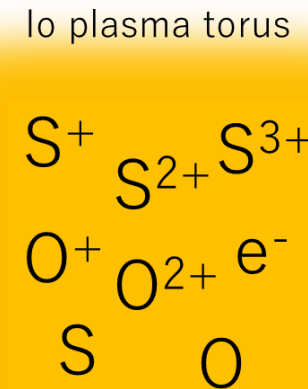
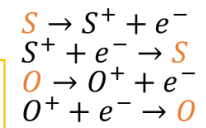
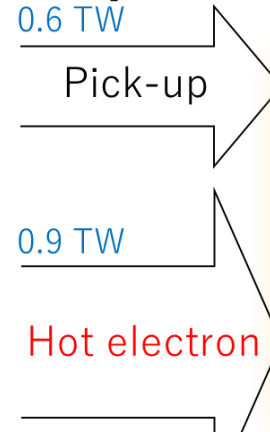


Fig. Electron velocity distribution at 5.5 R<sub>j</sub> from the center of Jupiter (Scudder, 1981)

$$E_{pickup} = \sum_{\alpha,\beta} k_{\alpha\beta} n_{\alpha} n_{\beta} T_{\beta} + \sum_{\gamma} I_{\gamma} n_{\gamma} n_e T_{\gamma}$$

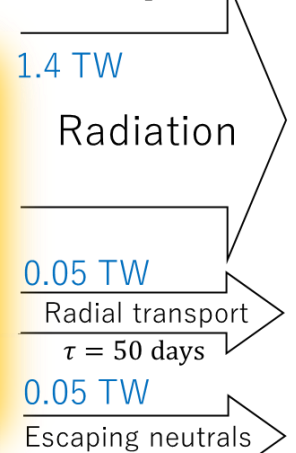


**Input**



$$E_{radiation} = \sum_{\beta,\gamma} \rho_{\beta,\gamma} n_e n_{\beta}$$

**Output**



$$E_{hot} = \sum_{\beta} v^{\beta/e} n_e (T_{\beta} - T_{\alpha})$$

Fig. Schematic diagram of energy budget in the IPT (values are derived by Bagenal and Delamere, 2011.)

$$E_{transport} = \sum_{\alpha} \frac{n_{\alpha} T_{\alpha}}{\tau}$$

# Radial transport with the interchange instability (I.I.)

Magnetic flux tubes will be exchanged if the total energy decreases by the interchange motion.

→ This mechanism could be effective to the transportation of hot plasmas in the outer region to the inner region.

The observational evidence has not been derived.

## Previous researches

### ■ Theoretical approach

The interchange unstable condition is expressed an inequality using the magnetic field, radial distribution of plasmas, and gravitational coefficient (Southwood and Kivelson, 1987).

### ■ MHD simulations (Hiraki et al., 2012)

### ■ In-situ observations (Russell et al., 2005)

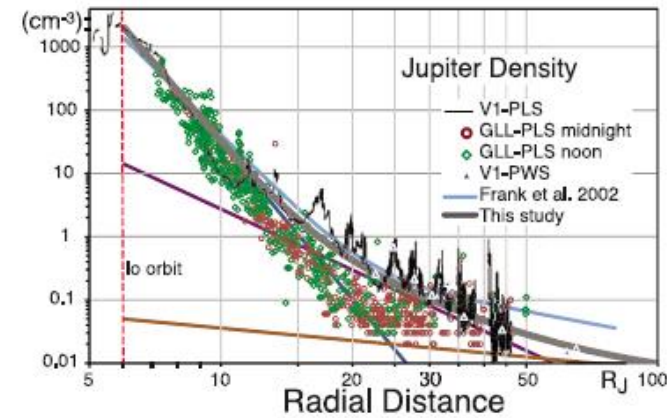


Fig. Radial distribution of plasma density in Jupiter's magnetosphere (Bagenal and Delamere, 2011)

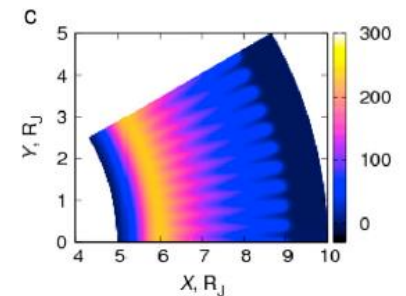
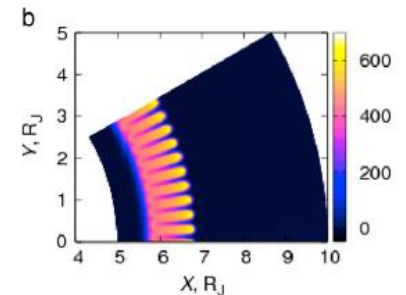
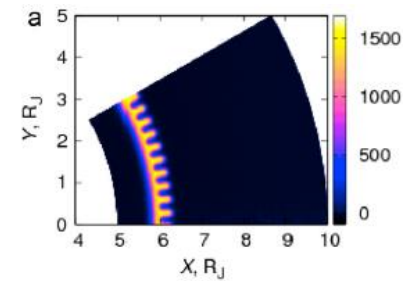


Fig. Simulation results about plasma flow with interchange instability (Hiraki et al., 2012)

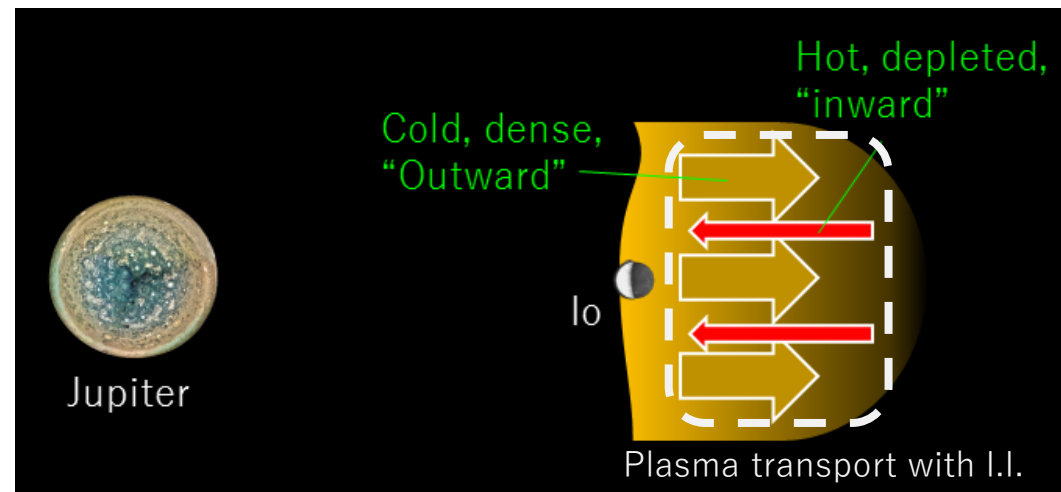


Fig. Schematic view of plasma radial transports with I.I. from polar view

# Purpose and Overview

- As to the interchange instability (I.I.) in the Jovian magnetosphere, some researches are based on the theoretical approach and MHD simulation, but **there is no research using the observation data and showing whether I.I. is influential on circulation of materials and energy or not.**
  - We used data obtained by Hisaki and focused **on the response to the change in the amount of plasma supplied to the magnetosphere** and explore the above problem.
- In this study, the radial distributions of plasma density and temperature were derived from the intensities of emission lines in the extreme ultraviolet range obtained by Hisaki.

# Used data obtained by Hisaki satellite

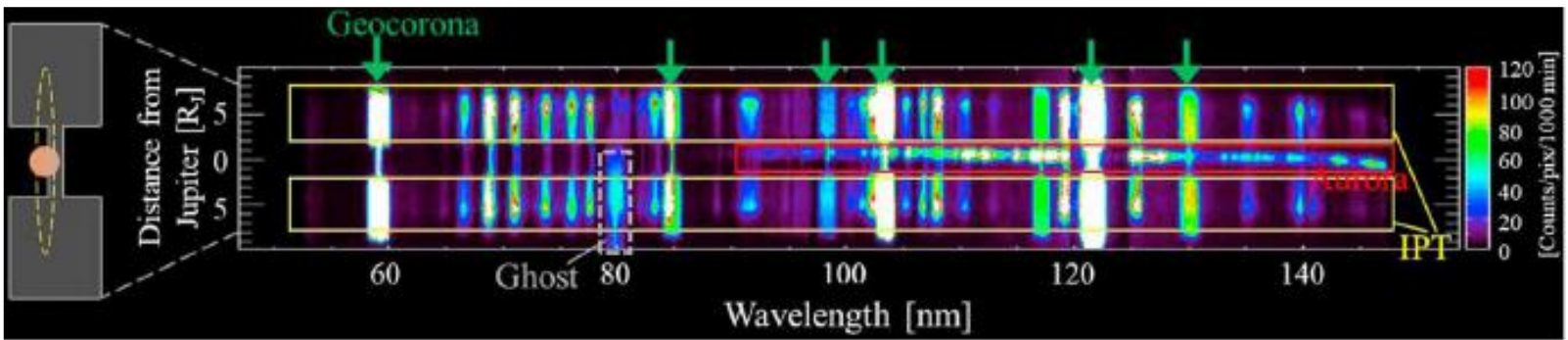


Fig. Spectral image of the IPT and aurora obtained using 140-arcsec slit with 2783-min integration

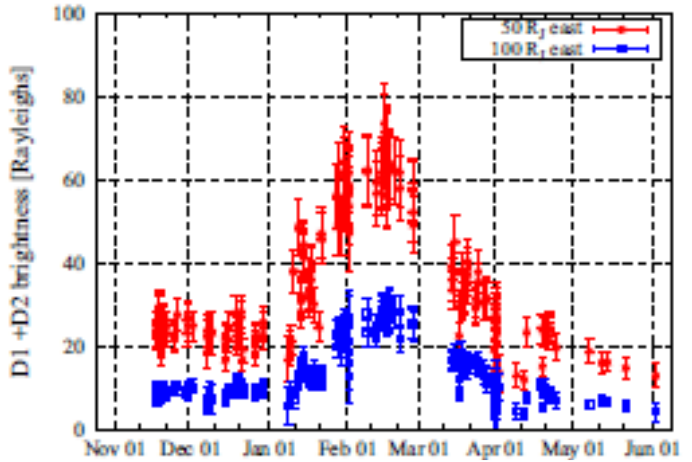


Fig. Variation in intensity of Na D line obtained by the ground observation (Yoneda et al., 2015)

- Wavelength range : 50-147 nm
- Spatial coverage : 7~8R<sub>J</sub> from the center of Jupiter
- Earth orbit (altitude: ~1000 km)
- Orbital period : 106 min.
- Slit type : 140-arcsec slit
- Observation period : 2013/11/30-Now

# In this presentation, we will introduce results from Nov. 2014 to May. 2015. In mid January 2015, activation of Io volcanoes was confirmed by the ground-based observations (Yoneda et al., 2015; De Kleer and de Pater, 2016).

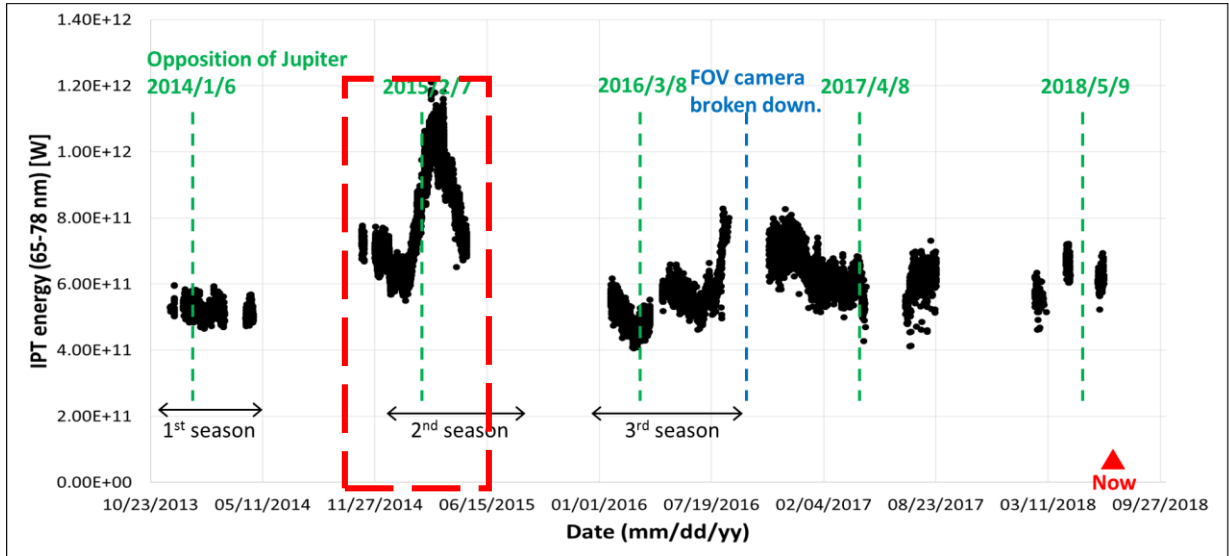
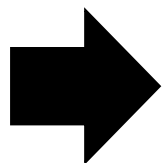


Fig. Time variation of IPT radiation captured by Hisaki observation

# Plasma diagnosis

The emission intensity of the emission line depends on the density of ions of the light emission source and the density and temperature of the electrons.

Dependence of electrons on density and temperature depends on emission lines.



From the intensities of multiple lines (remote observation data), the density of ions and the density / temperature of electrons (in-situ physical quantity) can be derived. In this study, the chi-squared minimum method was used for fitting to observation data and derive the parameters.

$$I(\lambda_{ji}) = \frac{1}{4\pi} \int N_j A_{ji} dl \text{ [photons/cm}^2\text{/sr/sec]}$$

$N_j$  : Ion density in energy state 'J'

Equilibrium equation between energy levels :

Natural transition probability

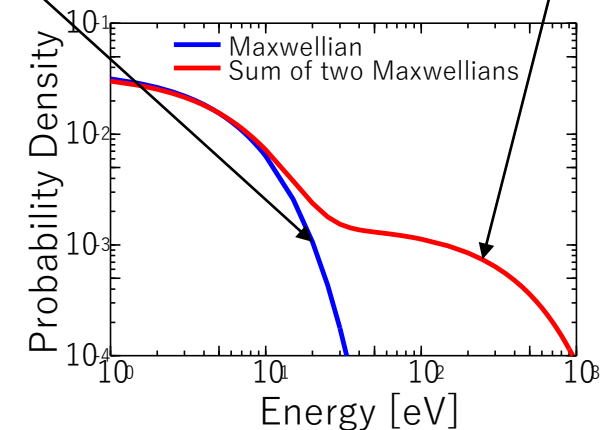
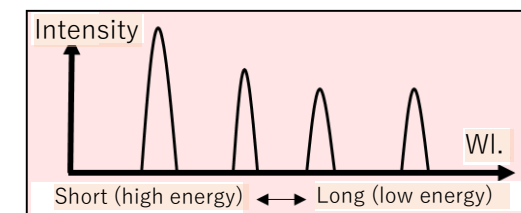
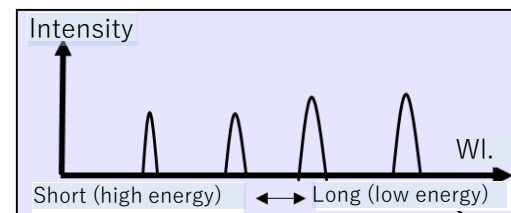
Collisional cross section

$$\alpha_{ij} = A_{ij} + N_e \int_0^\infty \widehat{g}_e v \sigma_e dv$$

※  $\widehat{g}_e$  : Electron velocity distribution

$$\begin{pmatrix} \alpha_{11} & \alpha_{21} & \alpha_{31} & \alpha_{41} & \cdot \\ \alpha_{12} & \alpha_{22} & \alpha_{32} & \cdot & \cdot \\ \alpha_{13} & \alpha_{23} & \cdot & \cdot & \cdot \\ \alpha_{14} & \cdot & \cdot & \cdot & \cdot \\ \cdot & \cdot & \cdot & \cdot & \cdot \end{pmatrix} \begin{pmatrix} N_1 \\ N_2 \\ \cdot \\ \cdot \\ \cdot \end{pmatrix} = \mathbf{0}$$

CHIANTI atomic database Ver. 8.0.7  
(Dere et al., 1979)



# Method for data analysis

## 1. Making spectra at each regions

- ✓ To integrate the spectroscopic images for 5 days.
- ✓ As to the oxygen line, we integrate images with the s/c local time limitation (20:00-4:00).
- ✓ To integrate the data covering ranges of projected radial distances from 5.9-6.3 R<sub>J</sub>, 6.3-6.7 R<sub>J</sub>, 6.7-7.1 R<sub>J</sub>, and 7.1-7.5 R<sub>J</sub> at dusk and dawn side respectively.

## 2. Calculating line intensities

- ✓ To fit spectra with gaussian functions and calculating line intensities.
- ✓ To use slit filling factor considering the torus width, distance between Earth and Jupiter, and instrumental function.

## 3. Plasma diagnosis

- ✓ To fit line intensities using CHIANTI atomic database Ver. 8.0.7.
- ✓ Column densities and temperature are derived.

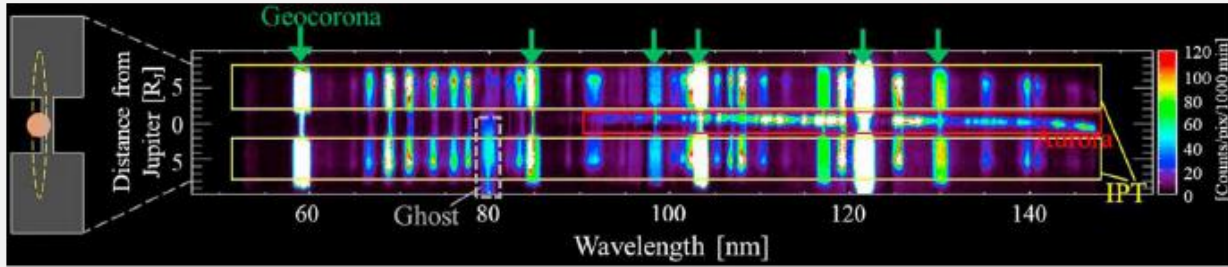
## 4. To calculate the radial profile of local values from the column densities and temperature assuming power-law function

- ✓ Chi-squared fitting was performed on the results of the plasma diagnosis in each region.
- ✓ Local values (N<sub>c</sub>, N<sub>h</sub>, N<sub>S</sub><sup>+</sup>, N<sub>S</sub><sup>2+</sup>, N<sub>S</sub><sup>3+</sup>, N<sub>O</sub><sup>+</sup>, and T<sub>c</sub>) are derived.

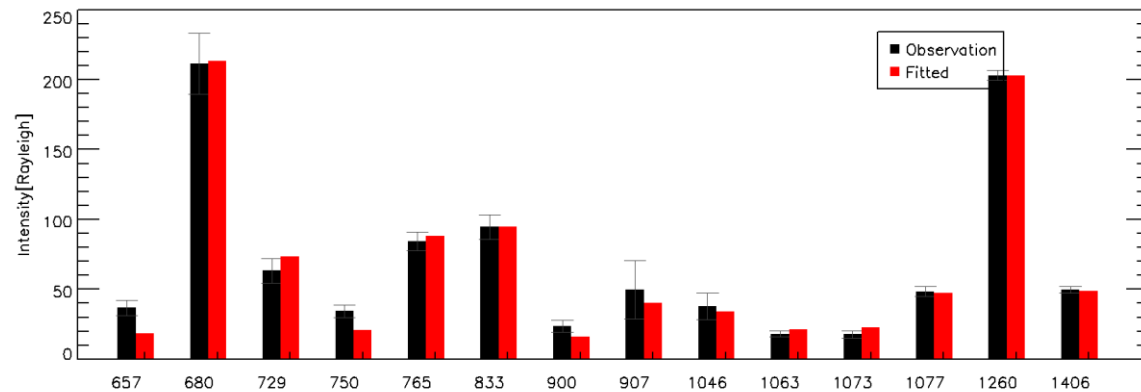
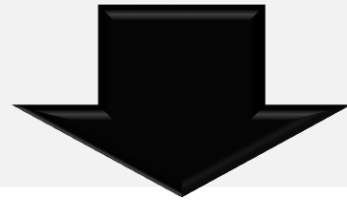
$$n(r) = n_0 \left( \frac{r}{r_0} \right)^7$$

( r<sub>0</sub>: 5.91 R<sub>J</sub> )

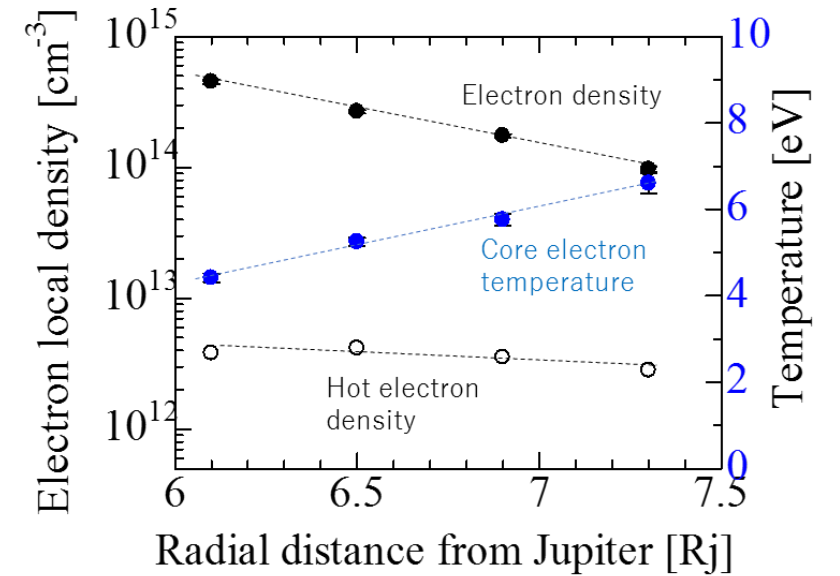
# Flow of data analysis



Example of spectroscopic image obtained by Hisaki



Example of spectrum



Example of radial distribution of column densities and temperature

# Assumptions

- The velocity distribution of electrons was taken as a sum of two Maxwellian distributions (Sittler and Strobel, 1987).
- $[H^+]/[e^-]$  was set at 0.1 (Bagenal, 1994).
- $[O^{2+}]/[O^+]$  was set at 0.1 (Steffl et al., 2004b).
- The hot electron temperature was set at 200 eV (Sittler and Strobel, 1987).
- Electrical neutrality was assumed.

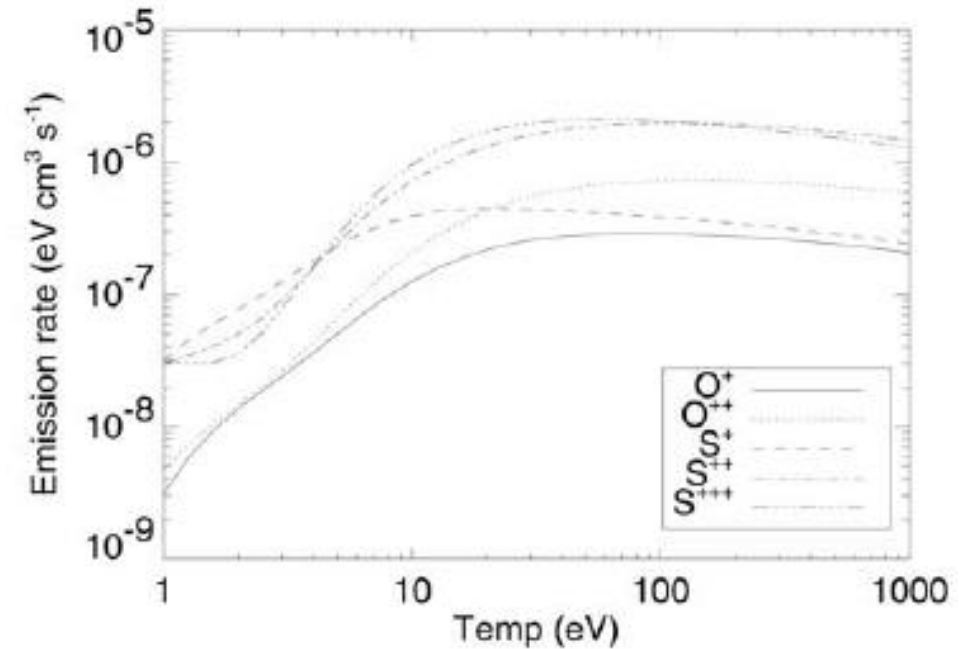


Fig. Emission rates (Ne=2000/cc)  
(Delamere and Bagenal, 2003)

# Results

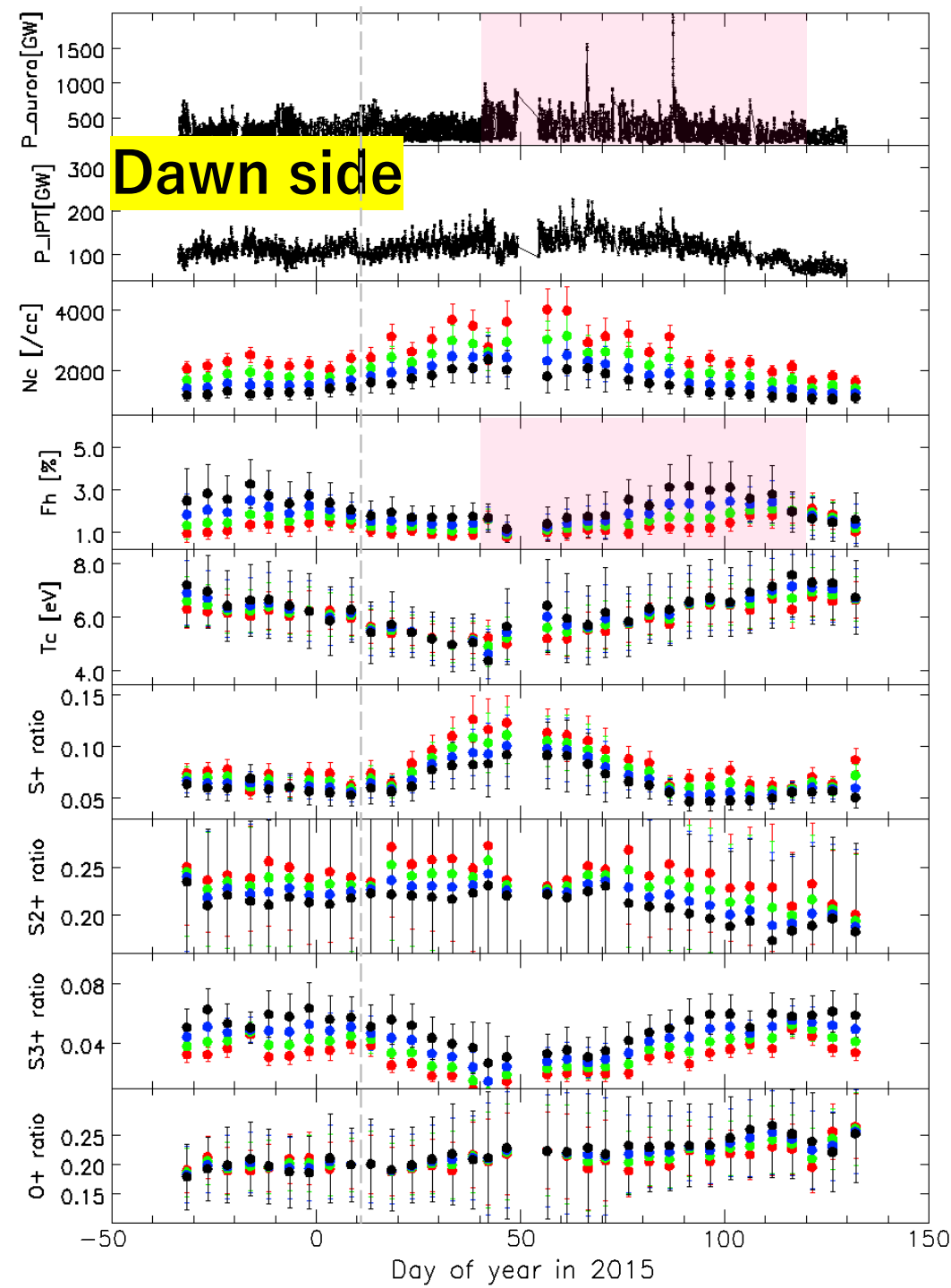
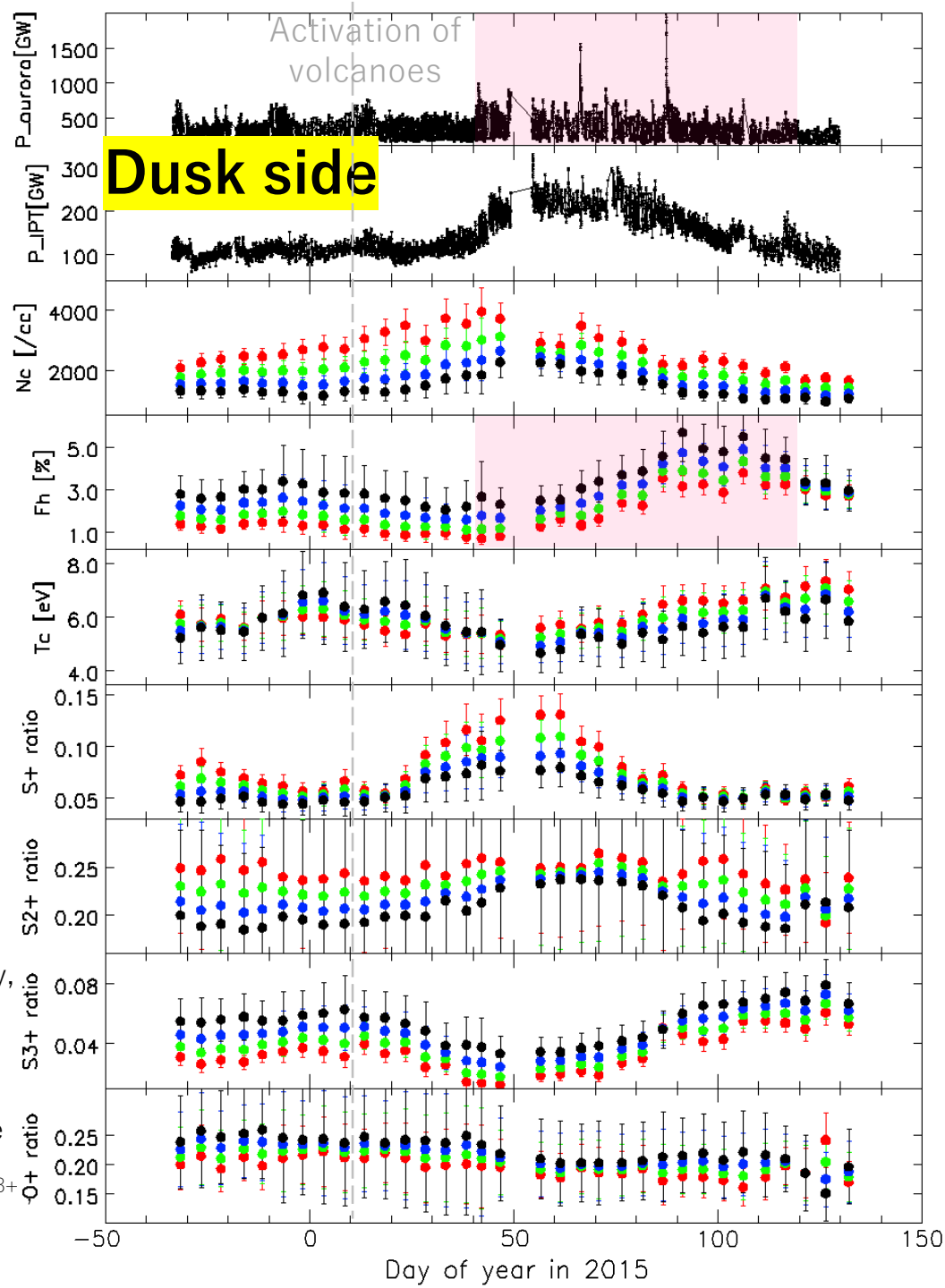
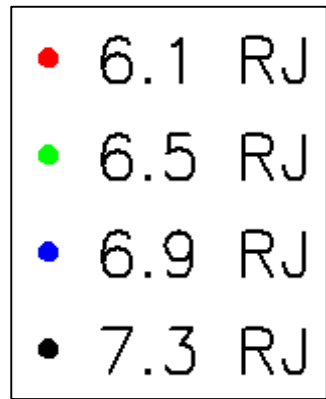


Fig. Time variation in auroral energy, IPT energy, and results of plasma diagnosis. From top, vertical axes show core electron density ( $N_c$ ), hot electron fraction ( $F_h$ ), core electron temperature ( $T_c$ ), mixing ratios ( $F_{S^+}$ ,  $F_{S^{2+}}$ ,  $F_{S^{3+}}$  and  $F_{O^+}$ ).

# Electron parameters

- The core electron density changed dynamically with the activation of volcanoes. On DOY ~50 in 2015, it was about twice the value at the quiet time.
- The hot electron fraction began to rise from DOY ~50 in 2015 and peaked at around DOY 85-120 in 2015. It peaked earlier in the outer region.
  - ⇒ The period during which the hot electron fraction was rising was almost the same as the period during which auroral activity was high. It is interpreted that the short-lived auroral brightening is caused by reconnection with mass loading (Kimura et al., 2018; Tsuchiya et al., 2018). Taken in this light, it is expected that **the increase in hot electrons is also caused by the active circulation in the radial direction.**
- The core electron temperature decreased to DOY ~50 in 2015 and then increased.
  - ⇒ The decrease/increase in core electron temperature seems to reflect the promotion of Coulomb relaxation of core/hot electrons due to the increase in core/hot electron density.

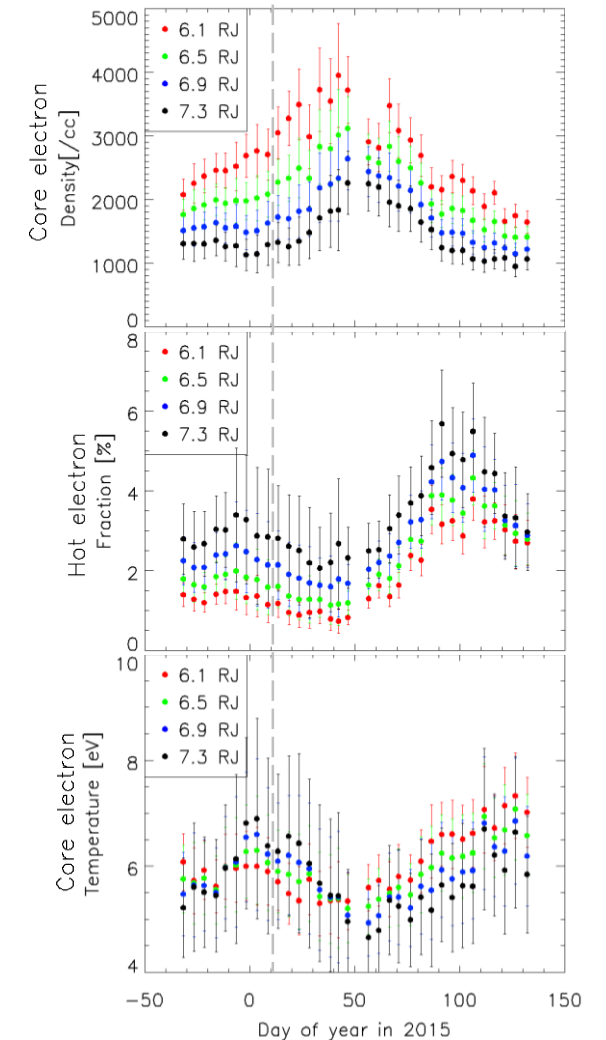


Fig. Time variation in core electron density ( $N_c$ ), hot electron fraction ( $F_h$ ), core electron temperature ( $T_c$ ).

# Examples of Spectra

- When the core electron density is its maximum (DOY 47 in 2015), almost all emission lines became bright.
- When the hot electron fraction is its maximum (DOY 101 in 2015), only emission lines in shorter wavelength range became bright.

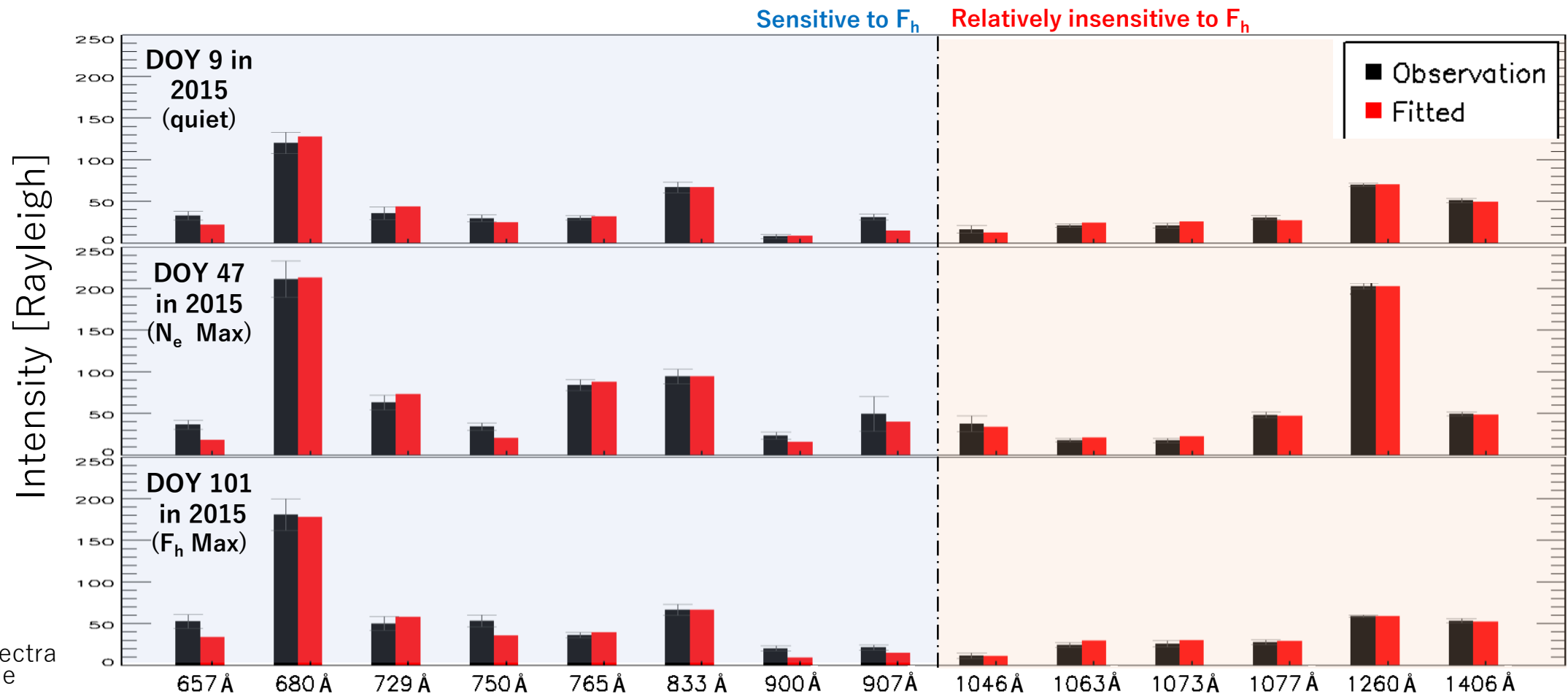


Fig. Examples of spectra at 6.1  $R_j$  at dusk side

# Ion parameters

■ The higher the valence number, the slower the peak timing of mixing ratio. The decrease in mixing ratio of  $S^{3+}$  after volcanic activation seems to reflect temporary promotion of the loss process of  $S^{3+}$  due to increase in sulfur atoms.

■ From the behavior of each parameter, it is suggested that a small-scale event of volcanic activation occurred even before DOY 10 in 2015.

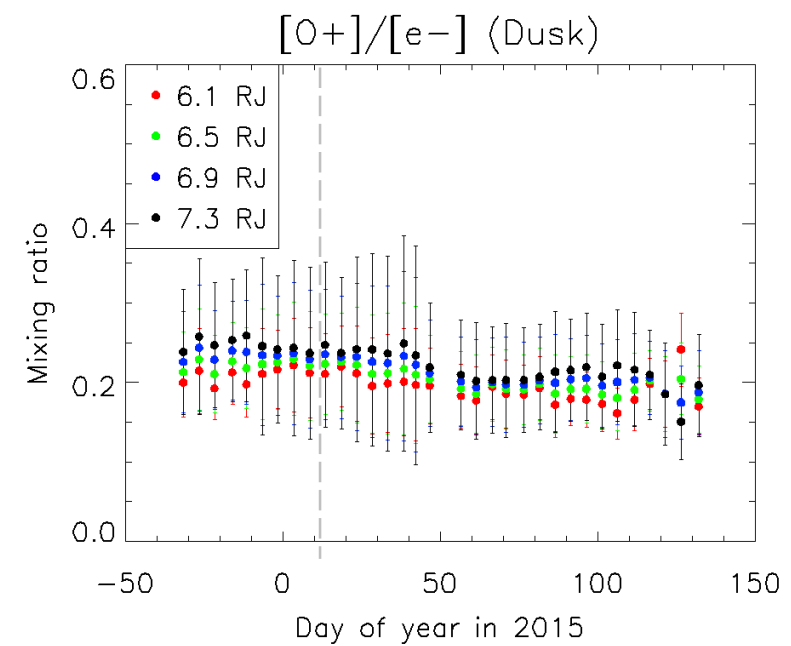
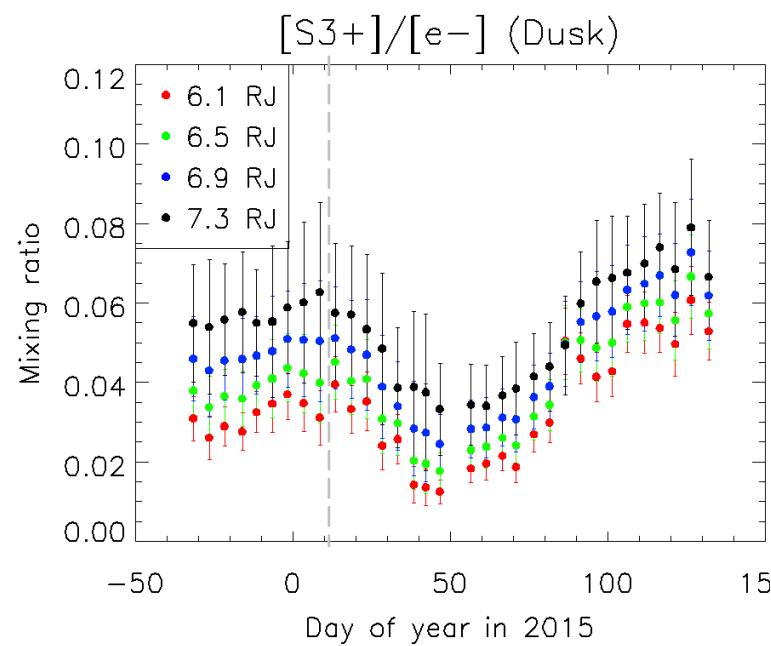
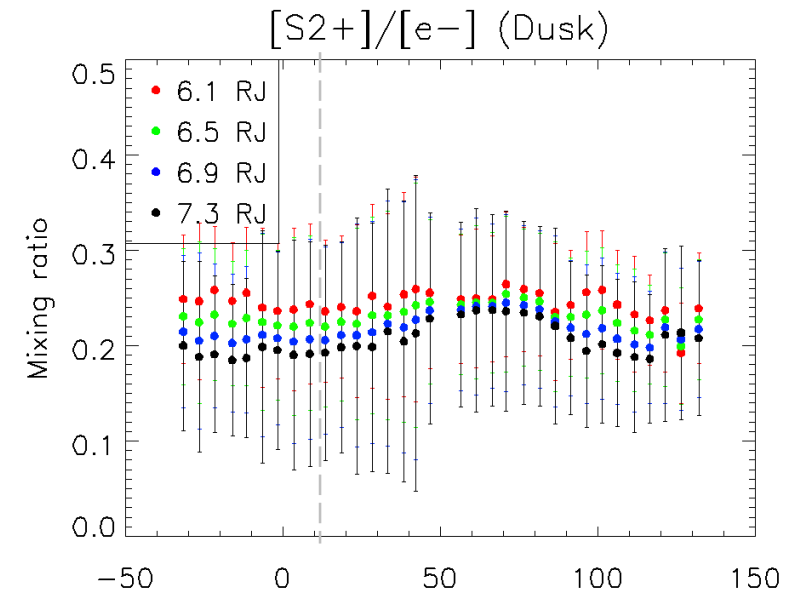
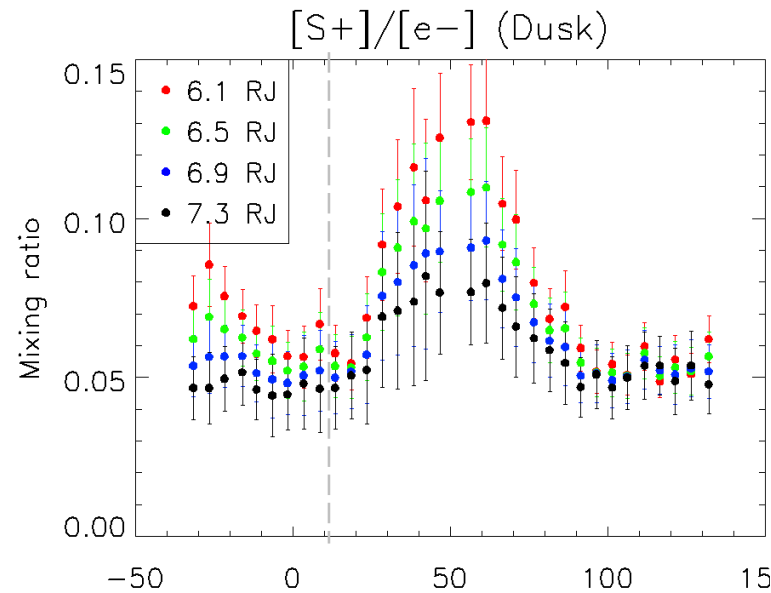


Fig. Time variation in mixing ratios ( $F_{S^+}$ ,  $F_{S^{2+}}$ ,  $F_{S^{3+}}$ , and  $F_{O^+}$ ).

# Comparison of dusk and dawn results

$N_c$  : On the dusk side, the peak is later in the outer area, but on the dawn side, the peak timing is almost independent of location

⇒ It suggests that the time scale for outward transport is shorter on the dawn side.

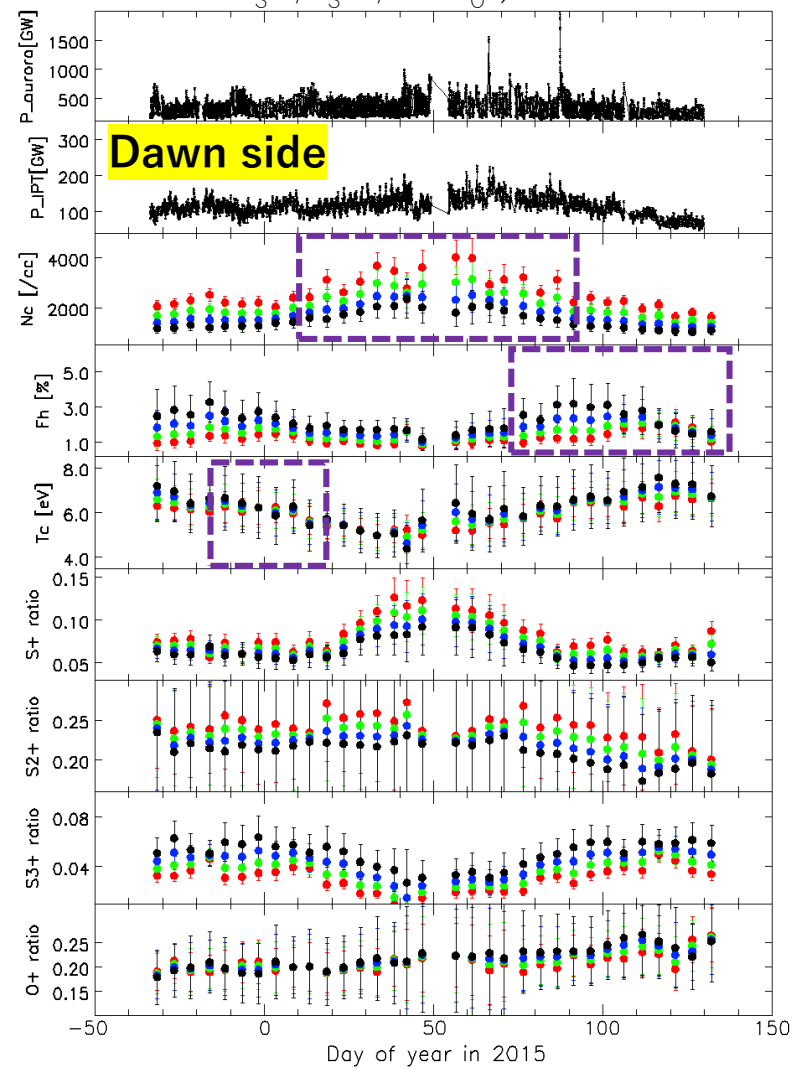
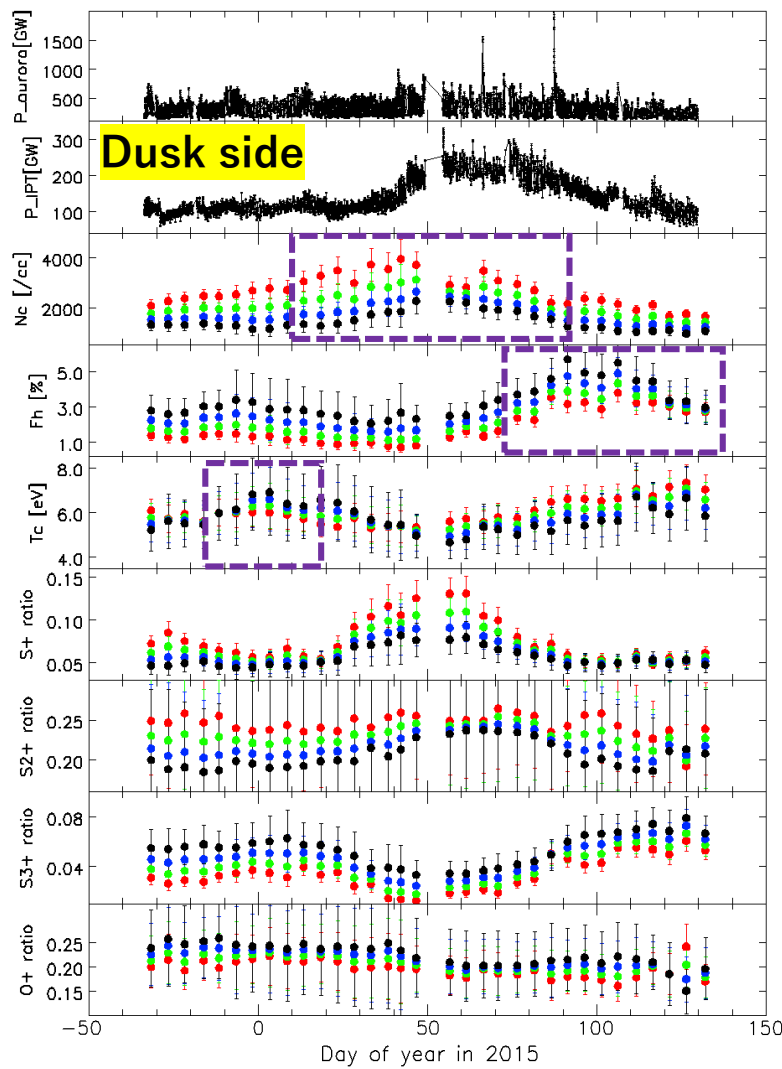
$F_h$  : The increase in  $F_h$  is more intense on the dusk side than on the dawn side.

⇒ Additional analysis is needed to interpret the results.

$T_c$  : On the dusk side, it has a local maximum point on DOY ~0 in 2015.

⇒ It seems to be caused by small volcanic event.

Fig. Time variation in auroral energy, IPT energy, and results of plasma diagnosis. From top, vertical axes show core electron density ( $N_c$ ), hot electron fraction ( $F_h$ ), core electron temperature ( $T_c$ ), mixing ratios ( $F_{S^+}$ ,  $F_{S^{2+}}$ ,  $F_{S^{3+}}$ , and  $F_{O^+}$ ).



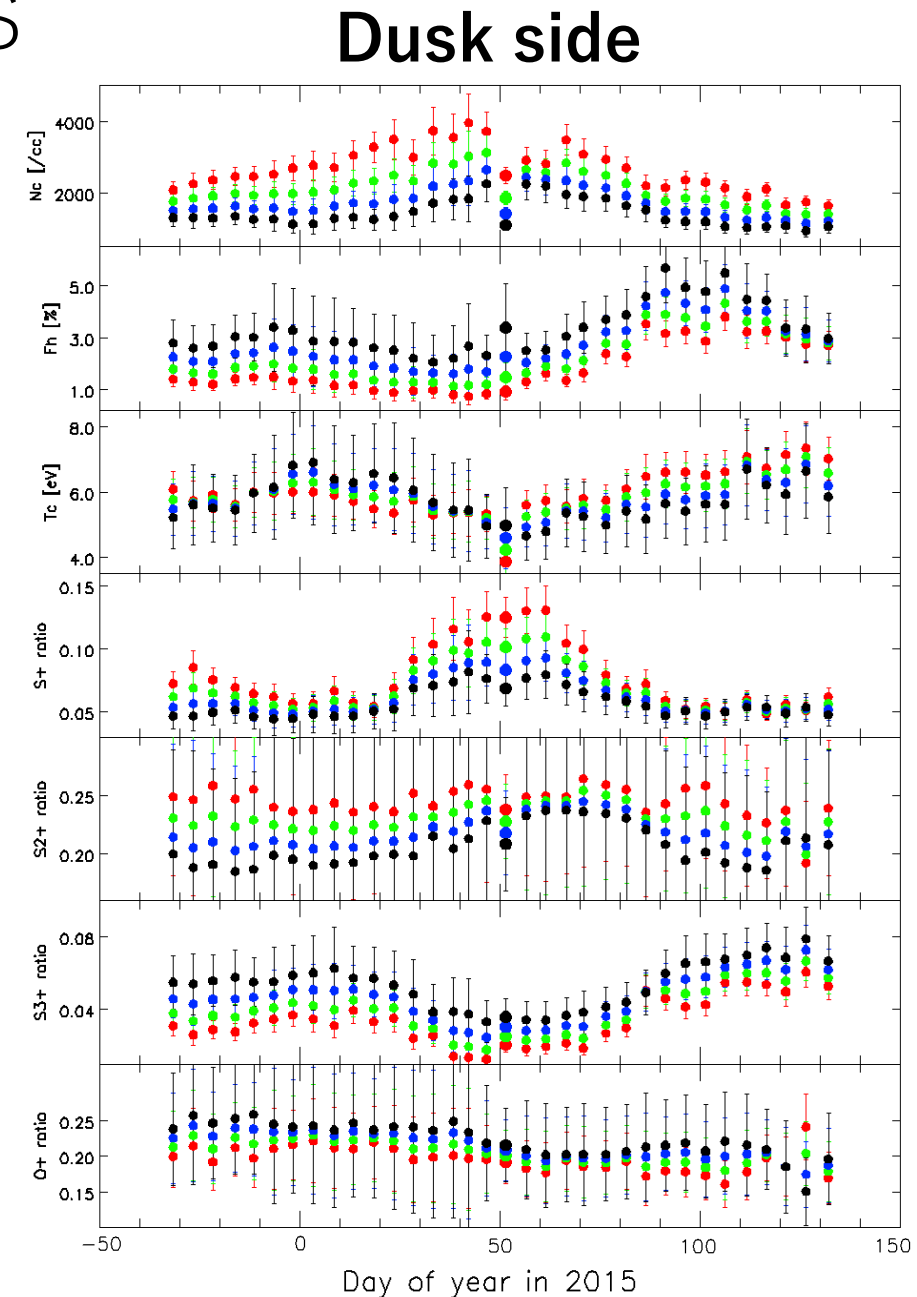
# Comparison with previous works

- Core electron temperature and mixing ratios are almost in agreement with the values derived by the previous researches ( $T_c \approx 5$  eV @6  $R_J$  and in table) (Bagenal, 1994; Steffl et al., 2004b; Yoshioka et al., 2017; Nerney et al., 2017).
- Also core electron density in the quiet period is almost in agreement with previous results ( $N_c \approx 2000$  @6  $R_J$ ) (Bagenal, 1994; Steffl et al., 2004b; Yoshioka et al., 2017). However, as for the active period, the density is  $\sim 1.5$  times higher than the previous results by Yoshioka et al., 2018 (indicated by large circles).
- The hot electron fraction is slightly higher than the values derived by some previous results (0.1-0.3 % in Delamere and Bagenal, 2003).

Table from Yoshioka et al., 2018

Ions	Hisaki (This Study)	Cassini [Steffl et al., 2004b]	Voyager [Nerney et al., 2017]
$S^+$	$0.05 \pm 0.01$	$\sim 0.05$	$\sim 0.06$
$S^{++}$	$0.23 \pm 0.05$	$\sim 0.2$	$\sim 0.2$
$S^{+++}$	$0.05 \pm 0.01$	$\sim 0.03$	$\sim 0.03$
$O^+$	$0.19 \pm 0.05$	$\sim 0.2$	$\sim 0.22$
$O^{++}$	$0.1 \times [O^+]$ (assumed)	$\sim 0.03$	$\sim 0.03$

Fig. Time variation in results of plasma diagnosis. From top, vertical axes show core electron density ( $N_c$ ), hot electron fraction ( $F_h$ ), core electron temperature ( $T_c$ ), mixing ratios ( $F_{S^+}$ ,  $F_{S^{2+}}$ ,  $F_{S^{3+}}$ , and  $F_{O^+}$ ). Large circles indicate the previous research by Yoshioka et al., 2018.



# Summary

- By applying plasma diagnosis to Hisaki data, we clarified the change in plasma density and temperature in each region of the IPT. It was confirmed that the hot electron fraction increases as plasma density increases. Also, the peak date is more preceding at outer regions than inner regions. Those results suggest that the increase in hot electrons is caused by the active circulation in the radial direction.
- The future work is to evaluate the efficiency of I.I., other transportation, and/or heating mechanisms quantitatively using the above results.

# Appendix.

## How to estimate the slit filling factor( $\mathbf{SFF}_{(t=t_1)}$ )

$$\mathbf{SFF}_{(t=t_1)} = \mathbf{SFF}_{(t=t_0)} \times \frac{H_{(t=t_1)}}{H_{(t=t_0)}} \times \frac{R_{(t=t_0)}}{R_{(t=t_1)}}$$

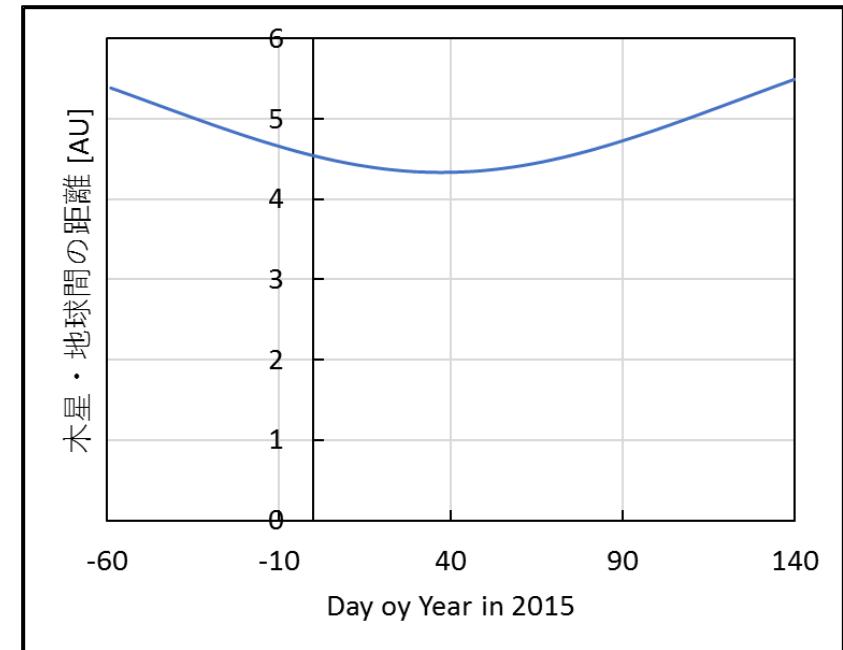
R: Distance between  
Jupiter and Earth

SFF: Slit filling factor

Estimated from data with 140-arcsec  
slit and 10-arcsec slit

H: Width of the emission region

# We conducted the analysis for typical lines of  
S II, SIII, SIV, and OII. When we calculate SFF, it  
was assumed that the width of the emission  
region is equal when the emitting species are the  
same.



Time variation in distance  
between Jupiter and Earth

# How to determine $SFF_{(t=t_0)}$ (SFF in Feb. 2015)

List of used lines

S IV 657
S IV 661
S III 680
S III 726, 729
S IV 750
S IV 754
S II 765
S III 897, 900
S II 907, 910
S II 1046
S IV 1063
S IV 1063
S III 1077
S II 1097
S II 1102
S II 1254
S II 1260
S IV 1406
S IV 1417

The width of torus image was evaluated by comparing the data with 140-arcsec slit and with 10-arcsec slit in the near term.

The fact that the value obtained by integrating the spectrum (wavelength vs. count rate) in the wavelength direction with the 140-arcsec slit was larger by the apparent width of torus than the case of 10-arcsec slit was utilized.

Date :

10-arcsec slit : 2015/2/18-2/22

140-arcsec slit : 2015/2/16-2/18, 2/23-2/25

# How to estimate the torus width of emission region ( $H$ )

Latitudinal structure of torus (to be wanted)

Instrumental function

$$f_{\text{Hisaki}} = f_{\text{torus}} * f_{\lambda} * f_{\text{inst}}$$

Obtained by Hisaki

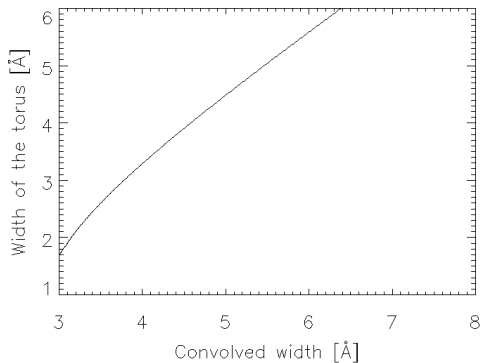
Structure of emission lines

$$H_{\text{torus},\lambda} = \sqrt{H_{\text{Hisaki}}^2 - H_{\text{inst}}^2}$$

FWHM obtained by Hisaki

Point spread function (FWHM)

- We assumed the point spread function (FWHM) of Hisaki/EXCEED at 76.5 nm as 1.89 Å.  
 ※ It was estimated by the torus width obtained by the T60 telescope with a high wavelength resolution.
- The point spread functions (FWHMs) at other wavelength was assumed by the above value at 76.5 nm and wavelength dependency of wavelength resolution (estimated from data with 10-arcsec slit).



## How to eliminate the effect of blend

Relationship between  $H_{\text{torus},\lambda}$  (with blend) and  $H_{\text{torus}}$  (without blend) was calculated using CHIANTI atomic database.